

https://doi.org/10.1070/QEL17978

Quantum optical magnetic field sensor for neurodiagnostic systems of a new generation

M.V. Petrenko, A.S. Pazgalev, A.K. Vershovskii

Abstract. **Magnetic encephalography is currently the most informative method of functional study of the brain, since, unlike other methods, it allows one to localise deep sources of biosignals and perform three-dimensional mapping of neuronal activity. The main factors hindering the development and spread of this method are the complexity and high cost of diagnostic tools, as well as the rigidity of the requirements they impose on the spatial and temporal uniformity of the magnetic field. The prospects for desinging a device capable of largely overcoming these limitations are considered. A review of studies aimed at developing an optical sensor applicable to magnetic encephalography is presented. The all-optical single-beam nonzero-field sensor proposed by the authors earlier is separately considered.**

Keywords: *optical magnetometer, atomic magnetometer, quantum sensor, optical pumping, magnetoencephalography.*

1. Introduction

Clarifying the principles of brain functioning is one of the most important scientific tasks interdisciplinary facing humanity. The study of the mechnism of higher nervous activity of humans and animals is at an early stage and requires the development of new methods for studying neuronal activity based on the registration of electric and magnetic fields of the brain. The main source of the magnetic field of biological objects is the conduction current that occurs during ion exchange in cell membranes. The strongest magnetic fields are due to muscle contraction: e.g., during a heartbeat, fields that reach 50–100 pT are generated on the body surface; these fields are examined by magnetocardiography (MCG) methods. Much weaker magnetic fields arise in the nervous system during the transmission of nerve impulses: e.g., in the cerebral cortex, weak magnetic fields from 10 fT to 1 pT are produced by electric currents flowing in neurons [1]. Magnetoencephalography (MEG) is a non-invasive method for studying the activity of neurons in the living human or animal brain. It is characterised by good spatial resolution (2–3 mm) and excellent temporal resolution, about 1.5 ms. This method has fundamental advantages over electroencephalography, since it allows deep sources of biosignals to be localised, and three-dimensional rather than surface mapping of neuronal activity to be performed. The high potential sensitivity of the method is due, in particular, to the fact that the magnetic permeability of the head tissues (both brain and bone tissues) practically does not differ from that of vacuum [2].

Since the 1960s, brain magnetic fields have been measured using multichannel superconducting quantum interference device (SQUID) gradiometers with a sensitivity of $1-3\ \mathrm{fT}/\sqrt{\mathrm{Hz}}$ [3]. Until the beginning of the 21st century, the high sensitivity of the SQUID magnetometers used to solve the problems of biomagnetism remained unsurpassed.

Optically pumped magnetometers [optical magnetometers (OMs), or atomic magnetometers] are another class of quantum electronic devices capable of measuring the magnetic fields of biological objects. The working substance in OMs is the vapour of alkali metal atoms or gaseous helium in a metastable state. Magnetometers using the principles of optical pumping and radio-optical double resonance were proposed by Dehmelt [4] and developed by Bell and Bloom [5]. Gradually, the sensitivity of optically pumped magnetometers reached [6] and surpassed [7] the sensitivity of SQUID magnetometers, and OMs began to be considered as an alternative to SQUID magnetometers in MEG systems. Optical magnetometers used in MEG systems can be conventionally divided into two classes: zero-field magnetometers capable of operating in fields not exceeding one to two hundred nanotesla (the scale here is set by the width of the magnetic resonance line or by the range of compensating coils built into the magnetometer), and nonzero-field OMs.

The first OMs were pumped with low-power gas-discharge lamps. The use of narrow-band single-mode semiconductor lasers for pumping and detecting magnetic resonance signals has significantly expanded the scope of OM applications and made it possible to increase their sensitivity. For MEG systems, evidence has now been obtained for the advantages of arrays of magnetometers with optical pumping over arrays of SQUID magnetometers in terms of performance, signal-to-noise ratio, overall information content, and achievable spatial resolution [8].

Let us take note of the main fundamental differences between the two systems for recording brain magnetic fields. Optically pumped magnetometers, in contrast to SQUIDs, do not require low helium temperatures; the sensitive element (cell) of an OM is heated to a temperature slightly higher than room temperature. The absence of a low-temperature thermostat (Dewar vessel) required for SQUID sensors and designed as a non-adaptive helmet, makes it possible to detect magnetic fields at a much shorter distance from their sources and, thereby, increase both the amplitude of the recorded signal and the spatial resolution. Optical magnetometers are placed on an easily manufactured helmet, adapted to the

M.V. Petrenko, A.S. Pazgalev, A.K. Vershovskii Ioffe Institute, ul. Politekhnicheskaya 26, 194021 St. Petersburg, Russia; e-mail: antver@mail.ioffe.ru

Received 19 October 2021; revision reeceived 13 December 2021
Kvantovaya Elektronika **52** (2) 119–126 (2022)
Translated by V.L. Derbov

physiological characteristics of the object, which allows bringing them as close as possible to the surface of the head.

SQUID magnetometer arrays require special magnetically shielded rooms to operate. The high cost and immobility of such rooms are the main factors hindering the widespread use of MEG methods for diagnosing brain diseases (note that these limitations are also inherent in zero-field OMs). Another factor is the cost of maintaining SQUID arrays that require liquid helium.

When using nonzero magnetic field atomic magnetometers, there are no magnetic field homogeneity requirements that make magnetically shielded rooms necessary. Nonzero-field magnetometers can be used in much simpler, more compact and cheap magnetic shields or even without magnetic shielding [9]. Despite the fact that the typical size of an OM sensor exceeds the size of a SQUID sensor, a significantly smaller number of OM sensors compared to the number of sensors in a SQUID array is sufficient for spatial signal localisation in the cerebral cortex [10].

For MEG systems, the OM sensor must have high sensitivity, small size, and high speed. The sensitivity should allow signals of 10–1000 fT to be recorded at a distance of 2–3 cm from the head surface. The area occupied by a separate sensor on the helmet should be 2–4 cm^2, and the distance between the sensors should not exceed 1.5–2 cm. The sensor cell should be located as close as possible to the source of the magnetic field. The speed of the sensor must be high enough to register the magnetic fields of the brain in the frequency band of 2–150 Hz (ideally, up to 600 Hz).

The sensors must not create mutual electromagnetic interference, and so an ideal solution is an all-optical sensor, in which the signal is excited and recorded optically without the use of resonant RF fields. In addition, such sensors must remain operational under magnetic interference, i.e., have a dynamic range that exceeds the magnitude of these interferences. This requirement is especially important for nonzero-field OMs operating in an unstable field (i.e., outside the shield). The use of sensors in a gradiometric configuration allows one to largely compensate for magnetic field disturbances caused by distant sources.

It should be noted that in recent decades there has been a clear trend towards miniaturisation of magnetic sensors and increasing their sensitivity at the expense of worsening absolute accuracy and stability of measurements. This is due not only to the advent of microminiature sources of optical pumping, but also to the attention of the developers of such devices changed from geological exploration to biology and medicine, because of the explosive growth of interest in MEG and MCG methods.

2. Optical magnetometers

Optically pumped magnetometers can be divided into two main classes: magnetometers using resonant excitation of the precession of magnetic moments (magnetic resonance) and magnetometers using a signal of the zero-field magnetic level crossing (Hanle effect) [11]. The Hanle effect, as applied to magnetometry, manifests itself in the fact that, as the magnetic field decreases to values at which the precession rate of magnetic moments turns out to be small compared to the rate of their relaxation, optical pumping causes a change in the refractive and absorption index of the medium. Therefore, magnetometers based on the Hanle effect operate in fields whose magnitude does not exceed the characteristic width of the magnetic resonance line, usually tens or hundreds of nanotesla. Such magnetometers can be designed according to a single-beam [12] or double-beam scheme [7]. In a double-beam scheme, one beam is used for pumping and the other for detection. Most often, detection in a double-beam scheme is implemented using linearly polarised light, detuned in frequency from the pump absorption line [13]. Hanle magnetometers typically use low-frequency modulation of the magnetic field in one or two perpendicular directions rather than RF fields. In the latter case, magnetometers can simultaneously record two magnetic field components perpendicular to the pump beam. The first magnetometer of this type was proposed in 1964 by E.B. Alexandrov et al. [14].

Among zero-field magnetometers, the highest sensitivity, exceeding that of SQUID magnetometers [15–17], is demonstrated by magnetometers using the spin-exchange relaxation free (SERF) regime [18, 19]. A commercial version of SERF magnetometers are QuSpin magnetometers [20]. The sensitivity of these devices in a zero field reaches $7-10$ fT/$\sqrt{\text{Hz}}$ with a sensor size of 12.4×16.6 mm. The maximum field value in which these devices remain operational is 200 nT (http://quspin.com).

Nonzero-field OMs provide an alternative to SERF sensors [21]. Their operation is based on magnetic resonance, i.e., the precession of the collective magnetic moment of atoms. The collective moment in the ground state of an atom is produced by polarised light, the frequency of which is resonant to the optical transition; this process is called optical pumping [22]. As a rule, circularly polarised light propagating along the magnetic field is used for pumping. Photons of such light carry an angular momentum, which is transferred to the atoms and creates the orientation of their magnetic moments (spins). The precession of the collective magnetic moment is excited and phased by a resonant periodic action of an external radio-frequency field or light, the parameters of which (intensity, frequency or polarisation state) are modulated at a certain frequency. The precession signal of the collective magnetic moment, i.e., the magnetic resonance signal, is recorded optically by measuring a change in the absorption or refraction of the transmitted light.

Nonzero-field magnetometers, in turn, can be divided into two subclasses. The first one includes magnetometers that record a signal proportional to the magnetisation component M_z produced by pumping along the magnetic field (hereinafter, we assume that the magnetic field vector is directed along the z axis of the Cartesian coordinate system). The main disadvantages of M_z magnetometers are, firstly, low speed and, secondly, high sensitivity to pump radiation noise. Both drawbacks arise because the signal in magnetometers is recorded at a low frequency, not exceeding the width of the magnetic resonance line. For these reasons, they have not yet been used to register MEG signals, although, as will be shown below, such attempts are still ongoing.

The second subclass includes M_x magnetometers (Fig. 1) that record the rotating (precessing) component of the magnetic moment transverse with respect to the field, more precisely, its projection M_x onto the x axis perpendicular to the field. In a nonzero magnetic field, the precession of the collective magnetic moment periodically modulates the parameters of light used to detect transverse magnetisation. The performance is limited only by the magnitude of the measured field. However, it should be taken into account that at frequencies exceeding the width of the magnetic resonance line $\Gamma = 1/T_2$ (T_2 is the relaxation time of the transverse component of the

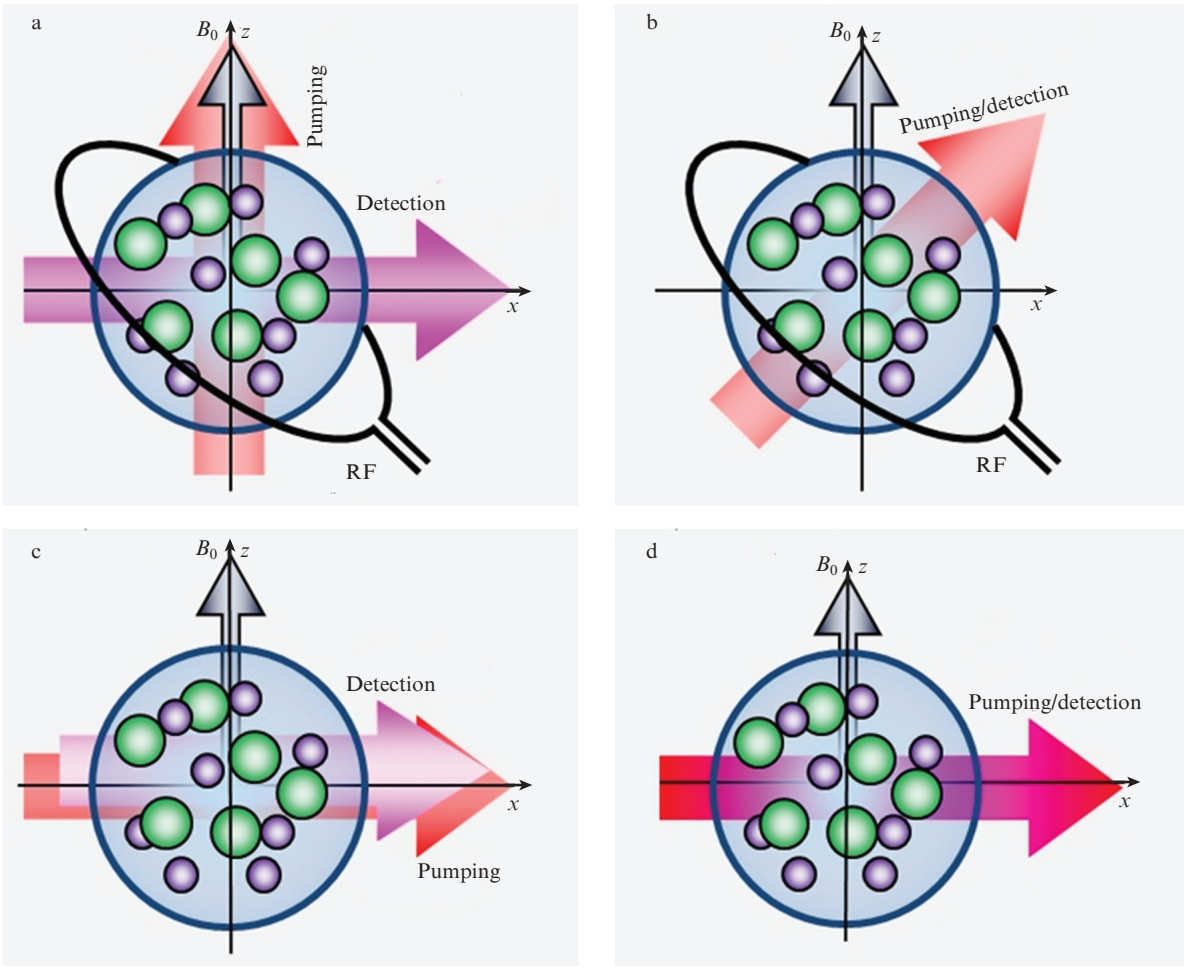

Figure 1. (Colour online) Various M_x magnetometer schemes: (a) classical double-beam circuit with a RF field, (b) its simplified single-beam version, (c) double-beam Bell–Bloom scheme, and (d) its single-beam version; B_0 is the external magnetic field.

magnetic moment), the sensitivity of M_x magnetometers decreases in proportion to the frequency.

The best sensitivity is provided by the double-beam scheme of an M_x magnetometer, in which one (longitudinal) beam performs pumping, and the other (transverse) one detects the resonance (Fig. 1a). It measures the rotation of the polarisation plane of a linearly polarised beam [23]. In this case, the probe beam, detuned in frequency from the optical absorption contour by many of its widths, does not perturb the magnetic resonance, and the rotation of the probe beam plane of polarisation is detected by a balanced photodetector, which makes it possible to largely suppress the noise of the probe laser radiation.

The single-beam scheme of the M_x magnetometer (Fig. 1b) is a simplified version of the double-beam scheme, in which a circularly polarised pump beam longitudinal with respect to the direction of the field vector is combined with a transverse circularly polarised probe beam into one beam directed at an angle of 45° to the magnetic field. This compromise allowed, at the expense of the loss of sensitivity, a significant simplification of the optical design and increase in the competitiveness of optical sensors. In the variants of M_x magnetometers listed above, the precession of the magnetic moment is excited by a resonant radio-frequency magnetic field. Bell and Bloom [24] suggested using the modulation of the parameters of light directed across the magnetic field as an alternative method for exciting induced precession (Figs 1c and 1d). Circularly polarised light modulated at the resonance frequency creates a nonzero collective transverse magnetic moment that precesses around the magnetic field vector. Initially, the variant of the optical scheme proposed in [24] was single-beam with detection of the absorption of a circularly polarised probe beam, but then it was replaced by a more efficient double-beam scheme (Fig. 1c).

The phase of the magnetic moment precession can be set using modulation of the amplitude, frequency, or polarisation state of the pump light [25]. Since the modulation of the pump light parameters in the spectral representation is equivalent to the appearance of coherent harmonics of the acting radiation component, the effect of such modulation can be considered in terms of coherent population trapping [26]. The undoubted advantage of the Bell–Bloom magnetometer scheme is that the resonance is excited without using radio-frequency fields, i.e., the sensor can be all-optical. The most commonly used is the double-beam version of the Bell–Bloom scheme with amplitude modulation of the pump light and detection of the transverse component by the second beam. The separation of beams is needed because in a single-beam scheme it is difficult to extract the magnetic resonance signal from the modulation signal. The compactness of a double-beam sensor can be ensured if the pump and detection beams pass through the cell along the same path, after which they are separated, e.g., using a dichroic mirror or an interference filter.

The single-beam version of the Bell–Bloom scheme (Fig. 1d) proposed by the authors of this review will be presented below.

3. Optical sensors for MEG

Zero-field magnetometers not subject to the destructive effects of spin-exchange relaxation (SERF) [7] were the first OMs that demonstrated a sensitivity sufficient for recording MEG signals (0.54 fT/$\sqrt{\text{Hz}}$ for a cell volume of 0.3 cm^3). A double-beam measurement scheme was used. The first magnetograms using the SERF technology [27] were also obtained in a double-beam scheme with orthogonal pump and detection beams. As mentioned above, such a scheme cannot provide the compactness of the sensor required to implement an array of a sufficiently large number of sensors. Therefore, in compact sensors, a single-beam scheme is used or two beams are directed along the same path.

Since 2016, the QuSpin zero-field sensors mentioned above have become commercially available, and in 2018 they began to be used in multichannel MEG systems. It has been shown that the OM array in such systems has clear advantages over SQUID arrays [8]. Thus, according to Ref. [28], an array of only eight QuSpin sensors provides higher information content than a system of hundreds of SQUID magnetometers, when measuring the activity of brain gamma rhythms in the range of 30–150 Hz.

Boto et al. [29] compared the results of the measurements of the cortical response to speech using an array of 45 OMs and an array of 275 SQUID magnetometers. The comparison showed a high (over 70%) degree of correlation of the results, which evidences in favour of high OM efficiency. According to the authors of Ref. [29], OM systems will ultimately replace cryogenic sensors in MEG systems.

Zero-field optical magnetometers were used [30] to demonstrate a non-invasive brain-computer interface (BCI). The possibility to send simple messages using signals read by OM was shown.

Using four sensors, Bu et al. [31] measured for the first time the magnetic signal from the median nerve to the wrist and showed that OMs make it possible to detect magnetic fields of moving peripheral nerves.

S. Knappe's group tested an array of 21 SERF gradiometers with a baseline of 2 cm [32] under zero-field conditions. The average sensitivity of the gradiometer sensor was 15 fT/$\sqrt{\text{Hz}}$ at a distance of ~4 mm between the sensor face and the center of the nearest cell. Nardelli et al. [32] noted that an array of gradiometers can be used in MEG systems in a magnetically noisy medium.

Pratt et al. [33] describe the Kernel Flux system, which contains 432 optically pumped magnetometers and is designed to visualise brain activity in a zero field. The helmet contains 48 units, each containing 9 SERF zero-field magnetometers arranged in a 3×3 matrix with a 5 mm step. The unit size is approximately 15×15 mm, and the cell size is approximately 2–3 mm. Each unit is pumped and interrogated by a separate laser, whose frequency is stabilised by means of the reference cell. The sensitivity of an individual magnetometer was measured in a magnetically shielded room and amounted to 80 fT/$\sqrt{\text{Hz}}$ at a frequency of 3 Hz, and the sensitivity averaged over a unit was 25 fT/$\sqrt{\text{Hz}}$. The sensors are designed to measure the magnetic field gradient in three directions.

Recently, interest has increased in the development of MEG systems capable of operating outside multilayer magnetic shields, and in general in the development of highly sensitive all-optical sensors operating in a nonzero field and having a sensitivity better than 100 fT/$\sqrt{\text{Hz}}$ [34]. Clancy et al. [35] simulated numerically the possibility of using OMs to visualise brain activity outside magnetic shields. The simulation results are verified in an experiment using a phantom virtual array simulating a magnetic dipole in a conducting sphere in a nonzero magnetic field. It is noted that since the existing small-sized nonzero-field magnetometers have a sensitivity of about 70 fT/$\sqrt{\text{Hz}}$, then an array of 128 sensors and signal averaging over at least 100 measurement cycles will be required to localise the characteristic source of neural activity of the cerebral cortex with an accuracy of 1 cm. In the case of increasing the sensitivity by at least an order of magnitude, i.e., up to 7 fT/$\sqrt{\text{Hz}}$, then for an array of 100 sensors over 100 measurements, the localisation uncertainty will decrease to 1 mm, provided that the position of the sensors is known with an accuracy of 0.5 mm.

Perry et al. [36] demonstrated a gradiometer with a base of 4 cm operating in a magnetic field of 22 μT. A $5 \times 5 \times 50$ mm cell is used, which is heated to a temperature of 130 °C, pumping is carried out by the D_1 line of rubidium. The detection beam frequency is detuned from the pump beam frequency by 40 GHz. The gradiometer is desined according to a double-beam scheme implemented in a common cell. The volume of the sensitive area of each gradiometer sensor is 35 mm^3. The detection beam is common to the two sensors, but passes through them in opposite directions, providing a gradient measurement. Pumping and detection are carried out in pulses: pumping once, and detection four times during the precession period. The gradiometer sensitivity of 15–20 fT/$\sqrt{\text{Hz}}$ has been achieved.

In the absence of magnetic shielding, the recording of the MEG signal was demonstrated in Ref. [9], where a gradiometer with a base of 3 cm recorded signals generated by the human brain in the Earth's field. A sensitivity of 16 fT/$\sqrt{\text{Hz}}$ was obtained in a magnetic field of 51.4 μT. Two rubidium cells $8 \times 8 \times 12.5$ mm in size were placed in an evacuated cell measuring $6.5 \times 1.8 \times 1.8$ cm. A double-beam scheme was used, and the free precession signal was recorded. The pump cycle was a few microseconds, and the detection cycle was 2.3 ms. The time of the MEG signal recording was 20 min, during which the brain was stimulated by sound signals. A gradient signal of ±100 fT/$\sqrt{\text{Hz}}$ cm^{-1} with a signal-to-noise ratio of ~100 was recorded after the averaging over 462 records.

The results of measuring the parameters of a rubidium gradiometer based on a single multipass cell, optically pumped by beams with opposite circular polarisations, are presented in Ref. [37]. The sensitivity of the gradiometer was measured to be 10 fT/$\sqrt{\text{Hz}}$ in a weak magnetic field. The gradiometer base is 14 mm. The size of the gradiometer (due to the fact that it is designed according to a double-beam scheme with orthogonal pump and detection beams) is $80 \times 40 \times 20$ mm with a cell size of $18 \times 20 \times 30$ mm. Lucivero et al. [37] expect that due to the direct subtraction of signals in a common cell, the gradiometer will be especially effective at suppressing broadband magnetic noise.

Guo et al. [38] proposed a compact sensor with a cell volume of 64 mm^3, which uses the effect of magnetic resonance line narrowing by pump light. The sensor operates in a nonzero field. Magnetic resonance is excited by a transverse radio-frequency field generated by special coils. The magnetic resonance is detected using the second beam by the rotation of the polarisation plane. The pump laser is tuned to the transi-

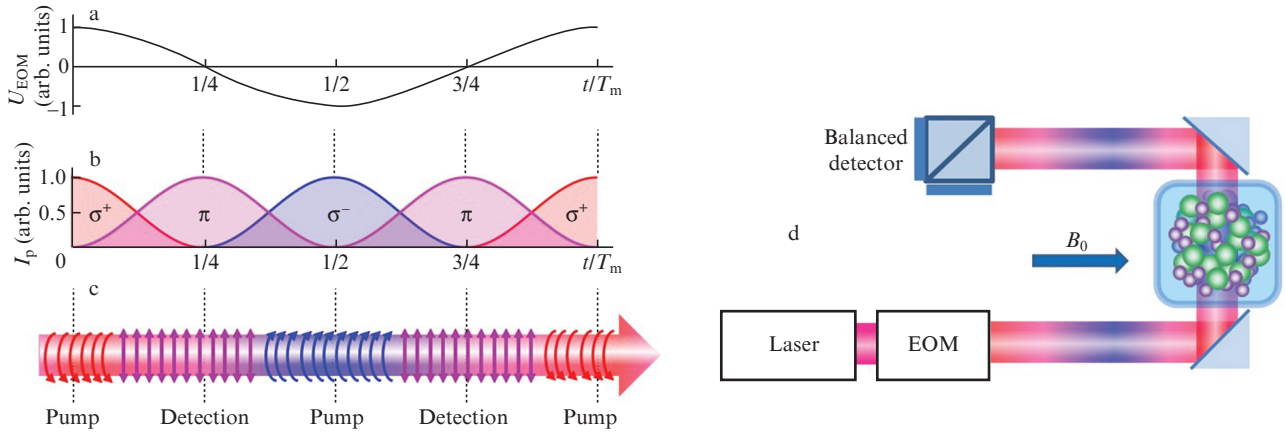

Figure 2. (Colour online) Modulation of the polarisation of the pump/detection beam: (a) variation of the control voltage U_{EOM} and (c, b) the corresponding changes in the intensities I_p of the (π; b) linear and ($\sigma^{\pm}$; c) circular components of the beam, as well as (d) the scheme of a single-beam quantum optical sensor with a nonzero magnetic field.

tion from the hyperfine level of the ground state with $F = 3$, as a result of which almost all atoms are pumped into a state with partially suppressed spin-exchange relaxation, which Happer [39] called the 'end-state', or 'stretched' state. Due to the partial suppression of relaxation, a sensitivity of 100 fT/$\sqrt{\text{Hz}}$ is achieved in a field of 10 μT. The sensor has a volume of ~100 cm^3 and is not all-optical.

Oelsner et al. [40] present an optically pumped caesium magnetometer for measurements in the Earth's magnetic field. The sensor operates in the mode of a balanced M_z gradiometer with oppositely directed circular polarisations of pump radiation in two channels [41]. The micromechanical unit, fabricated using the anode welding technique, contains two cells, each with a diameter of 5.5 mm and a thickness of 4 mm. The unit size is 35 × 35 × 6 mm, the linewidth is about 1.5 kHz, and the sensor bandwidth is several hundred hertz. A sensitivity of ~100 fT/$\sqrt{\text{Hz}}$ in the Earth's magnetic field of 50 μT has been demonstrated. The fundamental limit of sensitivity, limited by fundamental quantum noise, is 12 fT/$\sqrt{\text{Hz}}$. The size of the magnetometer sensor does not yet allow its use in MEG systems.

Zhang et al. [42] recorded the magnetic activity of the brain in the Earth's magnetic field using two magnetometers with cells 25 mm in diameter with an antirelaxation coating, constituting a gradiometer with a base of 6 cm. One of the magnetometers was used to stabilise the magnetic field in a system of magnetic coils with a diameter of about 4 m. The magnetometers were designed according to the double-beam Bell–Bloom scheme with resonance excitation by modulating the power of the pump light and recording the magneto-optical rotation of the detecting beam polarisation. The gradiometer demonstrated a sensitivity of ~4 fT/$\sqrt{\text{Hz}}$ cm^{-1}, which is sufficient for recording the brain alpha rhythm. Unfortunately, the size of the sensors does not allow them to be used in a multichannel MEG system.

Li et al. [43] present an atomic magnetometer implemented according to the Bell–Bloom scheme, operating in the geomagnetic range and using the linewidth narrowing effect. The authors consider a magnetically dependent transition between hyperfine levels of the ground state excited by modulation of the pump radiation frequency with the help of an electro-optical phase modulator (EOM) controlled by a microwave field. Pumping is carried out by circularly polarised light. The pumping and detection cycles are separated in time. The volume of the cesium cell is 64 mm^3. The sensitivity of the magnetometer is increased by pumping most of the atoms into a stretched state. As a result, spin exchange relaxation is suppressed and a sensitivity of 100 fT/$\sqrt{\text{Hz}}$ is achieved in a magnetic field of 10 μT. This magnetometer is designed according to a single-beam scheme, and its size is small enough for use in MEG systems.

Nonzero-field magnetometers significantly differ from SERF magnetometers: they are sensitive not to components of the field, but to its magnitude. Since in MEG systems the measurement of a weak signal of magnetic field variation is carried out against the constant background many times greater, it turns out that MEG sensors measuring the total field magnitude are sensitive only to the longitudinal component of the signal. On the one hand, this fact imposes restrictions on the applicability of such devices, and on the other hand, it allows the sensitivity axis of the sensor to be tilted by changing the external field direction. Petrenko et al. [44] developed a numerical algorithm for optimising an array of such sensors. They also presented the results of direct measurements of the sensitivity of two sensors in a gradiometric scheme: in the frequency domain free from acoustic noise, it was 13 fT/$\sqrt{\text{Hz}}$ per one sensor with a cell size of 8 × 8 × 8 mm (~0.5 cm^3). It was shown that this sensitivity is about 2.5 times lower than the ultimate sensitivity limited by the shot noise of light. This difference is mainly due to atomic projection noise, the effect of which was studied in [45] under conditions of resonance line narrowing by light.

4. Single-beam nonzero-field sensor for MEG systems

In this section, we briefly describe the scheme of a single-beam sensor, which was first proposed and studied by us in [46]. At present, this scheme (Fig. 1d, Fig. 2d) is the simplest version of the Bell–Bloom scheme, and at the same time the only one that allows using a single pump and detection beam, achieving maximum sensitivity limited by atomic projection noise.

In contrast to the schemes considered above, in our scheme the pumping and detection processes are separated in time, more precisely in phase, within one modulation period.

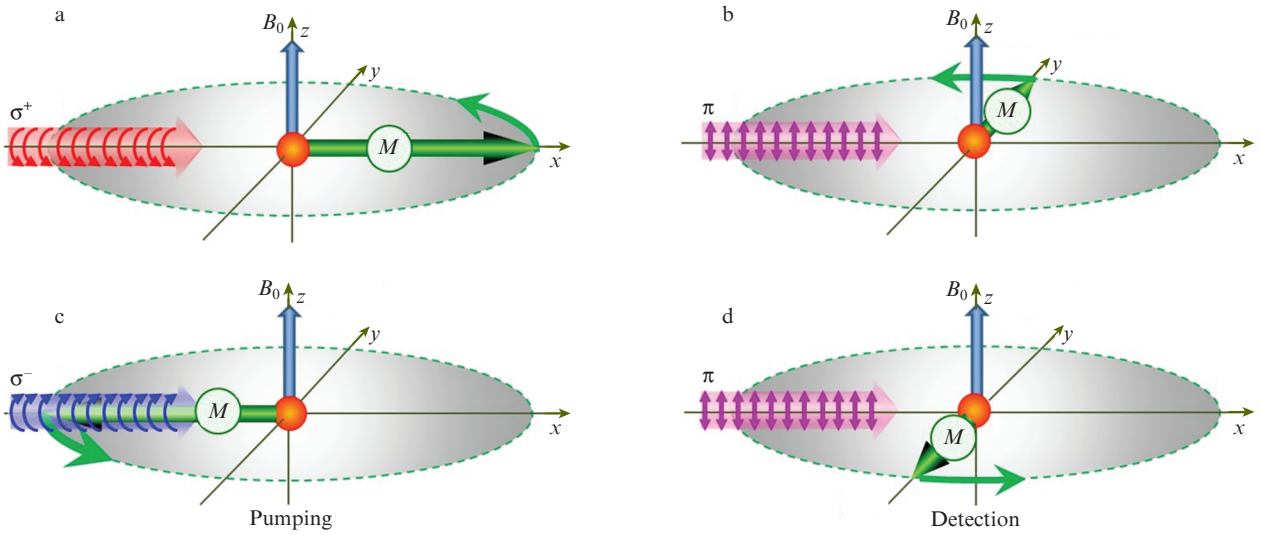

Figure 3. (Colour online) Phases of (a, c) pumping and (b, d) magnetic resonance detection; M is the magnetic moment.

In this case, one laser beam performs the functions of optical pumping, excitation, and detection of the magnetic resonance. For this purpose, we proposed changing the beam ellipticity E (in units of the phase delay between orthogonal linearly polarised components) with a frequency ω_m close to the Larmor frequency ω_0 from –45° to +45°, i.e., from the left circular polarisation to the right one (Figs 2a–2c). It is this type of modulation that is achieved with an EOM if its axes are oriented at an angle of ±45° to the polarisation azimuth of the incoming beam and an alternating (linear or sinusoidal) voltage of the appropriate amplitude is applied to it. When the control voltage passes zero, the ellipticity E is zero, which corresponds to the linear polarisation of the beam. Thus, during the period $T_m = 2\pi/\omega_m$, the beam polarisation becomes twice purely circular (σ^+ or σ^-) and twice purely linear (π) (Fig. 2). The circular components of the beam implement optical pumping and phasing of the precession of magnetic moments, while the linear component detects the magnetic resonance. Figure 2d shows a schematic of a single-beam sensor.

Effective pumping in the Bell–Bloom scheme occurs when the collective magnetic moment of the atomic ensemble is directed along the circularly polarised pumping beam (Figs 3a and 3c). It is no less important, however, that detection is carried out with maximum efficiency in the phase when the collective magnetic moment is perpendicular to the beam (Figs 3b and 3d). This is because the value of circular birefringence is proportional to the projection of the collective magnetic moment on the probe beam direction, and it is in this precession phase that the probe beam is particularly sensitive to the phase delay of the collective moment precession. This allows switching the pump and detection functions of the beam without loss of sensitivity.

The laser beam is tuned to a frequency close to that of optical transitions from the level with $F = I - 1/2$ of the ground state $S_{1/2}$ to the level with $F' = I \pm 1/2$ of the excited state of the alkali metal. In our experiment, we used Cs, but the proposed method is applicable to other alkali metals such as Rb and K. As shown in [47] and theoretically substantiated in [48], such a beam can simultaneously perform both Zeeman and hyperfine pumping due, firstly, to the partial overlap of the optical contours and, secondly, to the conservation of the nuclear component of the angular momentum in the optical excitation and relaxation cycle (Fig. 4). As a result, most of the atoms are assembled in an extended state at the level with $F = I + 1/2$ and $m_F = F$, in which the spin exchange rate can significantly decrease.

Note that the scheme shown in Fig. 4 corresponds to the case of 'classical' pumping by a beam propagating along the magnetic field. A complete interpretation of the case of pumping by a transverse beam is more complicated, it requires a transition from the laboratory xyz coordinate system (also used in Fig. 3) to the $x'y'z$ coordinate system rotating around the z axis with the Larmor frequency. As follows from the Bloch equations, the effective external magnetic field in such a system is zero, there is no Zeeman splitting of energy levels, the magnetic resonance frequency is also zero. If in this case the atoms are affected by a beam that is stationary in the $x'y'z$ system (i.e., rotating in the laboratory coordinate system xyz), then this beam could perform optical pumping of the medium without any modulation of its parameters.

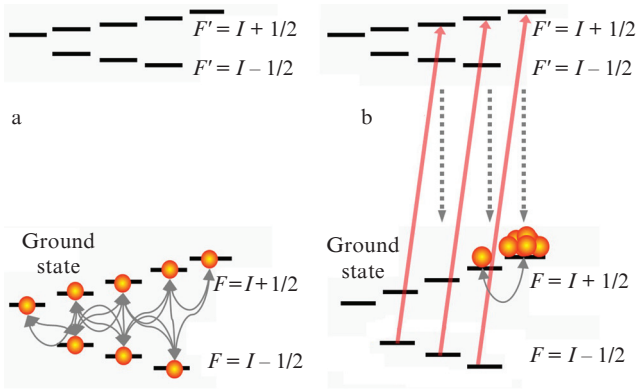

Figure 4. (Colour online) Energy level diagrams of an alkali atom (a) in thermal equilibrium and (b) under strong laser pumping by circularly polarised light at the frequency of optical transitions ($F = I - 1/2$) ↔ ($F' = I \pm 1/2$). Solid red arrows show optical pumping, dotted arrows show relaxation from the excited state to the ground state, and bidirectional gray arrows show spin-exchange relaxation.

However, in all existing versions of the Bell–Bloom scheme, use is made of the beams that are fixed in the laboratory coordinate system xyz. For considering the direction of the wave vector of such a beam constant in the rotating frame $x'y'z$ and, in the absence of other preferred directions, using it as the quantisation axis, this beam must be switched on in time periods corresponding to the same precession phase, i.e., it must be modulated at the Larmor frequency.

Despite such a difference between the Bell–Bloom scheme and the classical scheme, our experiments confirm that, as the intensity of the pump light increases, the (linear at this intensity) broadening of the magnetic resonance line is preceded by its narrowing, including the case of pumping with transverse modulated light [49].

The pump/detection beam deplets the level with $F = I - 1/2$ and makes the optical medium more transparent. Since the atoms are concentrated in the state with $F = I + 1/2$ and $m_F = F$, the probe π-component of the beam predominantly detects resonance at the level, from which it is detuned in frequency by nearly the hyperfine splitting of the ground state (for Cs this is 9.192 GHz). Thus, the conditions for quantum nondemolition (QND) measurement are realised. Hence, we simultaneously achieve almost optimal conditions for both optical pumping and detection.

Of course, the probe component of the beam also detects magnetic resonance at the level with $F = I - 1/2$. However, first, this level is almost completely depleted by optical pumping, and second, the resonance line due to the atoms occupying it is so strongly broadened by pumping light (a typical broadening value is tens of kilohertz) that the resonance manifests itself only as a wide and low pedestal.

It should be noted that since the intensity of the π-component of the beam is modulated at a frequency of $2\omega_m$, the third harmonic appears in the signal in addition to the first one. In the case of linear phase modulation, the amplitudes of the x-components of the first and third harmonics are respectively 3/4 and 1/4 of the signal value in the scheme using an unmodulated probe beam. The third harmonic of a signal can be measured and used in the same way as the first one.

Symmetric triangular modulation of the EOM control voltage gives rise to sinusoidal modulation of the ellipticity of the radiation polarisation. Optimal, as shown in [46], is the amplitude of about 1/3 of the amplitude that provides the range of ellipticity E from $-45°$ to $+45°$. The maximum sensitivity (less than 10 $\mathrm{fT}/\sqrt{\mathrm{Hz}}$ according to the estimated ratio of the resonance steepness to shot noise) is achieved at high (~95 °C) temperatures in an $8 \times 8 \times 8$ mm cell containing Cs and a buffer gas (N_2) and at a pump intensity of ~100 mW cm^{-2}. When the temperature is lowered to 70 °C, the sensitivity worsens by a factor of four to five, but the optimum in terms of pump intensity also decreases to a few mW cm^{-2}. This means that low-power vertical cavity surface emitting lasers (VCSELs) can be used in this regime.

Certain technical problems can arise when propagating a beam with modulated polarisation parameters through an optical fiber, since polarisation-maintaining fibres may not maintain the phase relationships of orthogonal eigenmodes. In this case, the EOM can be located at the output of the optical fibre, in close proximity to the sensor. However, even in this case, the exclusion of the second laser from the scheme provides much greater simplicity and, as a result, the compactness of the sensor.

5. Conclusions

This paper provides an overview of the current state of studies aimed at the development of nonzero-field sensors for MEG systems. Particular attention is paid to a recently proposed scheme in which optical pumping, excitation, and magnetic resonance detection are performed by a single laser beam with time-modulated ellipticity.

Acknowledgements. The section 'Single-beam nonzero-field sensor for MEG systems' was supported by the Russian Foundation for Basic Research (Research project No. 19-29-10004).

References

1. Hämäläinen M., Hari R., Ilmoniemi R.J., Knuutila J., Lounasmaa O.V. *Rev. Mod. Phys.*, **65**, 413 (1993).
2. Dash D., Ferrari P., Borna A., Iivanainen J., Schwindt P.D.D., Wang J. *Proc. 2021 10th Int. IEEE/EMBS Conf. on Neural Engineering (NER)* (Italy, 2021).
3. Cohen D. *Science*, **175**, 664 (1972).
4. Dehmelt H.G. *Phys. Rev.*, **105**, 1924 (1957).
5. Bell W.E., Bloom A.L. *Phys. Rev.*, **107**, 1559 (1957).
6. Alexandrov E.B., Balabas M.V., Pasgalev A.S., Vershovskii A.K., Yakobson N.N. *Laser Phys.*, **6**, 244 (1996).
7. Kominis I.K., Kornack T.W., Allred J.C., Romalis M.V. *Nature*, **422**, 596 (2003).
8. Iivanainen J., Stenroos M., Parkkonen L. *NeuroImage*, **147**, 542 (2017).
9. Limes M.E., Foley E.L., Kornack T.W., Caliga S., McBride S., Braun A., Lee W., Lucivero V.G., Romalis M.V. *Phys. Rev. Appl.*, **14**, 011002 (2020).
10. Boto E., Meyer S.S., Shah V., Alem O., Knappe S., Kruger P., Fromhold T.M., Lim M., Glover P.M., Morris P.G., Bowtell R., Barnes G.R., Brookes M.J. *NeuroImage*, **149**, 404 (2017).
11. Kastler A. *Nucl. Instrum. Methods*, **110**, 259 (1973).
12. Shah V., Knappe S., Schwindt P.D.D., Kitching J. *Nature Photonics*, **1**, 649 (2007).
13. Happer W., Mathur B.S. *Phys. Rev. Lett.*, **18**, 577 (1967).
14. Alexandrov E.B., Bonch-Bruevich A.M., Khodovoy V.A. https://rusneb.ru/catalog/000224_000128_0000176976_19651201_A1_SU/ (1964).
15. Sheng D., Li S., Dural N., Romalis M.V. *Phys. Rev. Lett.*, **110**, 160802 (2013).
16. Burghoff M., Sander T.H., Schnabel A., Drung D., Trahms L., Curio G., Mackert B.-M. *Appl. Phys. Lett.*, **85**, 6278 (2004).
17. Schmelz M., Zakosarenko V., Chwala A., Schönau T., Stolz R., Anders S., Linzen S., Meyer H. *IEEE Trans. Appl. Supercond.*, **26**, 1 (2016).
18. Happer W., Tam A.C. *Phys. Rev. A*, **16**, 1877 (1977).
19. Happer W., Tang H. *Phys. Rev. Lett.*, **31**, 273 (1973).
20. Shah V.K., Wakai R.T. *Phys. Med. Biol.*, **58**, 8153 (2013).
21. Bloom A.L. *Appl. Opt.*, **1**, 61 (1962).
22. Happer W. *Rev. Mod. Phys.*, **44**, 169 (1972).
23. Budker D., Gawlik W., Kimball D.F., Rochester S.M., Yashchuk V.V., Weis A. *Rev. Mod. Phys.*, **74**, 1153 (2002).
24. Bell W.E., Bloom A.L. *Phys. Rev. Lett.*, **6**, 280 (1961).
25. Grujić Z.D., Weis A. *Phys. Rev. A*, **88**, 012508 (2013).
26. Alzetta G., Gozzini A., Moi L., Orriols G. *Nuovo Cimento B*, **36**, 5 (1976).
27. Xia H., Ben-Amar Baranga A., Hoffman D., Romalis M.V. *Appl. Phys. Lett.*, **89**, 211104 (2006).
28. Iivanainen J., Zetter R., Parkkonen L. *Human Brain Mapping*, **41**, 150 (2020).
29. Boto E., Hill R.M., Rea M., Holmes N., Seedat Z.A., Leggett J., Shah V., Osborne J., Bowtell R., Brookes M.J. *NeuroImage*, **230**, 117815 (2021).
30. Wittevrongel B., Holmes N., Boto E., Hill R., Rea M., Libert A., Khachatryan E., Van Hulle M.M., Bowtell R., Brookes M.J. *BMC Biology*, **19**, 158 (2021).

31. Bu Y., Borna A., Schwindt P., Zeng X., Baum E., Rao R., Kimball D., Shah V., Coleman T., Huang M., Lerman I. bioRxiv 2021.05.18.444539 (2021).
32. Nardelli N.V., Perry A.R., Krzyzewski S.P., Knappe S.A. *EPJ Quantum Technol.*, **7**, 11 (2020).
33. Pratt E.J., Ledbetter M., Jiménez-Martínez R., Shapiro B., Solon A., Iwata G.Z., Garber S., Gormley J., Decker D., Delgadillo D., Dellis A.T., Phillips J., Sundar G., Leung J., Coyne J., McKinley M., Lopez G., Homan S., Marsh L., Zhang M., Maurice V., Siepser B., Giovannoli T., Leverett B., Lerner G., Seidman S., DeLuna V., Wright-Freeman K., Kates-Harbeck J., Lasser T., Mohseni H., Sharp T.J., Zorzos A., Lara A.H., Kouhzadi A., Ojeda A., Chopra P., Bednarke Z., Henninger M., Alford J.K. *Proc. SPIE*, **11700**, 1170032 (2021). DOI: 10.1117/12.2581794.
34. Fu K.-M.C., Iwata G.Z., Wickenbrock A., Budker D. *AVS Quantum Sci.*, **2**, 044702 (2020).
35. Clancy R.J., Gerginov V., Alem O., Becker S., Knappe S. arXiv:2105.02316 [physics] (2021).
36. Perry A.R., Bulatowicz M.D., Larsen M., Walker T.G., Wyllie R. *Opt. Express*, **28**, 36696 (2020).
37. Lucivero V.G., Lee W., Dural N., Romalis M.V. *Phys. Rev. Appl.*, **15**, 014004 (2021).
38. Guo Y., Wan S., Sun X., Qin J. *Appl. Opt*., **58**, 734 (2019).
39. Appelt S., Ben-Amar Baranga A., Young A.R., Happer W. *Phys. Rev. A*, **59**, 2078 (1999).
40. Oelsner G., IJsselsteijn R., Scholtes T., Krüger A., Schultze V., Seyffert G., Werner G., Jäger M., Chwala A., Stolz R. arXiv: 2008.01570 [physics] (2020).
41. Schultze V., Schillig B., IJsselsteijn R., Scholtes T., Woetzel S., Stolz R. *Sensors*, **17**, 561 (2017).
42. Zhang R., Xiao W., Ding Y., Feng Y., Peng X., Shen L., Sun C., Wu T., Wu Y., Yang Y., Zheng Z., Zhang X., Chen J., Guo H. *Sci. Adv*., **6**, eaba8792 (2020).
43. Li S., Zhang Y., Tian Y., Chen J., Gu S. *J. Appl. Phys*., **130**, 084501 (2021).
44. Petrenko M.V., Dmitriev S.P., Pazgalev A.S., Ossadtchi A.E., Vershovskii A.K. *IEEE Sensors J.*, **21**, 18626 (2021).
45. Vershovskii A.K., Dmitriev S.P., Kozlov G.G., Pazgalev A.S., Petrenko M.V. *Tech. Phys*., **65**, 1193 (2020) [*Zh. Tekh. Fiz*., **90**, 1243 (2020)].
46. Petrenko M.V., Pazgalev A.S., Vershovskii A.K. *Phys. Rev. Appl.*, **15**, 064072 (2021).
47. Scholtes T., Schultze V., IJsselsteijn R., Woetzel S., Meyer H.-G. *Phys. Rev. A*, **84**, 043416 (2011).
48. Popov E.N., Bobrikova V.A., Voskoboynikov S.P., Barantsev K.A., Ustinov S.M., Litvinov A.N., Vershovskii A.K., Dmitriev S.P., Kartoshkin V.A., Pazgalev A.S., Petrenko M.V. *JETP Lett*., **108**, 513 (2018) [*Pis'ma Zh. Eksp. Teor. Fiz.*, **108**, 543 (2018)].
49. Vershovskii A.K., Pazgalev A.S., Petrenko M.V. *Tech. Phys. Lett*., **46**, 877 (2020) [*Pis'ma Zh. Tekh. Fiz*., **46**, 43 (2020)].